The origin of non-thermal X-ray filaments and TeV emission in young SNRs

M. Lyutikov[1]

Physics Department, McGill University, 3600 rue University, Montreal, QC, Canada H3A 2T8

M. Pohl

Department of Physics and Astronomy, Iowa State University Ames, Iowa 50011-3160, USA

lyutikov@physics.mcgill.ca; mkp@iastate.edu

ABSTRACT

At the early, ejecta dominated, stage of supernova remnant (SNR) expansion a fraction of the swept-up circumstellar magnetic field is dynamically compressed to approximate equipartition at the contact discontinuity separating the SN progenitor's wind (or the ISM) and the ejecta. We propose that the thin non-thermal X-ray filaments observed by the Chandra satellite in several young SNRs are associated with such "pile-up" of the magnetic field. We use a one-dimensional diffusion-convection transport equation to describe the propagation of non-thermal electrons near the contact discontinuity of a young SNR and to calculate spatially resolved emission spectra in the X-ray and TeV bands. The results suggest that the high-energy electrons are possibly accelerated at the forward shock, and emitting efficiently only when they diffuse into regions of high magnetic field near the contact discontinuity. Much more likely, though, is that they are locally accelerated at the contact discontinuity, in which case the acceleration cannot be related to Fermi-type processes and should occur due to other plasma mechanisms. As a consequence, the forward shock in young SNRs is inconspicuous and often unobservable, similar to that in the Crab nebular.

1. Introduction

A number of young supernova remnants (SNRs) produce non-thermal X-ray emission (SN 1006, Koyama *et al.* 1995; Cas A, Allen *et al.* 1997; RX J1713.7-3946, Koyama *et al.* 1997; RCW 86, Borkowski *et al.* 2001, Bamba *et al.* 2000, Rho *et al.* 2002; G266.2-1.2, Slane *et al.* 2001). Recent high resolution Chandra observations of these SNRs indicate that a large fraction of the

[1]Canadian Institute for Theoretical Astrophysics, 60 St. George, Toronto, Ont, M5S 3H8, Canada

non-thermal X-ray emission is produced in very thin structures in the outer regions of the remnants (Cas A, Gotthelf *et al.* 2001; SN 1006, Bamba *et al.* 2001; RX J1713.7-3946, Uchiyama *et al.* 2003). The filament thickness is smaller than one tenth of a parsec, and possibly as small as one hundredth of a parsec.

In addition to X-rays, most prominent non-thermal SNRs show TeV-scale γ-ray emission (SN 1006, Tanimori *et al.* 1998; RX J1713.7-3946, Muraishi *et al.* 2000; Cas A, Aharonian *et al.* 2001a; see also the review by Vink 2004). Though the CANGAROO TeV γ-ary detections of SN 1006 and RX J1713.7-3946 are not confirmed to date, the overlap between the two populations is notorious: all TeV SNRs show non-thermal X-ray emission. The origin of the TeV emission is been currently debated. It has been attributed either to IC scattering of CMB photons by high energy electrons or to the decay of π^0 during interaction of the cosmic rays accelerated at the forward shock with ambient material (Berezhko, Ksenofontov, & Völk 2002, Berezhko, Pühlhofer, & Völk 2003).

The overall properties of the non-thermally emitting X-ray SNRs are quite different (Pannuti *et al.* 2003). SN 1006 was produced by a Type Ia SN, while RX J1713.7-3946 and Cas A are the result of core-collapse Type II SNe. SN 1006 is expanding into a low density environment, while Cas A and RX J1713.7-3946 are expanding into a wind blown cavity (Chevalier & Oishi 2003; Slane *et al.* 2001). We suggest that the uniting property is that these are young *pre-Sedov* SNRs (also non-plerionic). The reason why this may influence the non-thermal X-ray emission is that in the *pre-Sedov* phase the magnetic field is compressed to near equipartition values at the contact discontinuity separating the ejecta and the circumstellar medium. This may create suitable conditions for an efficient electron acceleration *at the contact discontinuity*.

The extreme narrowness of the filaments poses several problems for their interpretation. Conventionally, electrons are assumed to be accelerated at the forward shock by Fermi acceleration, in a way similar to cosmic rays. The non-thermal X-ray emission in the SNRs is generally thought to be synchrotron emission from electrons that have been accelerated to hundreds of TeV at the forward shock (see, though, Vink and Laming (2003) for a nonthermal bremsstrahlung interpretation). However, there are a number of problems that one encounters when trying to associate the narrow non-thermal filaments with acceleration at the forward shock.

- If the magnetic field is just the compressed ISM field, then the synchrotron decay times are usually too long to account for the narrow filaments. To reproduce thin filaments, the required magnetic field should be very high, of the order of equipartition with $B \sim 0.1 - 1$ mG, so that X-ray emitting electrons would lose most of their energy before they are advected or diffuse away from the filaments.

- The acceleration of electrons at the forward shock should produce a precursor in the upstream region of the shock. In the cleanest case of SN 1006 this is not seen with a very low upper limit (Long *et al.* 2003).

- In RCW 86 the detection of a strong Fe K_α line by Rho *et al.* (2002) showed that it cannot

be produced by thermal emission from a cosmic-abundance plasma, but it can be produced by Fe-rich ejecta. Similar conclusions has been reached by Bamba *et al.* (2003) for the case of SN 1006. (Please note again that SN 1006 was caused by a Type Ia SN.) These observations seem to exclude acceleration at the forward shock, for there is no heavy element enhancement around the forward shock.

- The acceleration efficiency required to explain the very high energy synchrotron cut-offs (above 10 keV) is too high for shock drift acceleration (*e.g.* Uchiyama *et al.* 2003 in case of SNR RX J1713.7.3946). [1]

- Attempts at the broadband (X-ray through TeV γ-ray) modeling of SNR emission has encountered difficulties. This is exemplified by the best studied case of RX J1713.7-3946. Initially, Enomoto *et al.* (2002) concluded that the TeV spectrum is a good match to that predicted by pion decay, and cannot be explained by other mechanisms. This was questioned by Reimer & Pohl (2002) and Butt *et al.* (2002), who concluded that the pion-decay model adopted by Enomoto *et al.* (2002) is in conflict with the existing data. They argued that, though RX J1713.7-3946 is accelerating electrons to super TeV energies, no convincing evidence for hadron acceleration exists to date. Finally, Pannuti *et al.* (2003) found that neither non-thermal bremsstrahlung nor neutral pion decay can adequately describe the TeV emission. On the other hand, the synchrotron-inverse Compton model can reproduce the data with magnetic field 150 μG, but the derived ratio of volumes for TeV emission and X-ray emission (approximately 1000) was deemed too large (see also Lazendic *et al.* 2004).

In attempt to resolve these contradictions, Berezhko, Ksenofontov, and Völk (2002; 2003) suggested that very efficient acceleration of cosmic-ray nucleons may indeed cause near-equipartition magnetic fields on account of streaming instabilities near the forward shock (McKenzie & Völk 1982; Lucek & Bell 2000; Bell & Lucek 2001). In this case, the relative fluctuation amplitudes of the magnetic field have to be much larger than unity, $\delta B/B \gg 1$, the cosmic-ray diffusion should be in the Bohm limit, and the total energy density in cosmic rays and in the magnetic field are of the order of equipartition. If the magnetic field is that high and is homogeneous over the remnant, the total magnetic energy would be similar to the expansion kinetic energy of the remnant. These are seriously constraining conditions. Also, the non-detection of TeV-scale gamma-ray emission from shell-type SNRs in a high-density environment does not support the notion of cosmic-ray nucleons acceleration to energy densities at the equipartition level (Buckley *et al.* 1998; Aharonian *et al.* 2001b, 2002).

[1] In the framework of the diffusive shock acceleration model, the synchrotron cutoff energy is set by the condition acceleration rate = synchrotron loss rate. The diffusive shock acceleration time is $t_{acc} \sim 10\kappa/V^2$, where $\kappa = \eta r_L c/3$ is the diffusion coefficient in the upstream region, and V is the upstream velocity of the shock, $\eta \geq 1$ is the gyrofactor. The maximum energy of synchrotron emission is then $\epsilon_X = 2(V/2000 kms^{-1})^2/\eta$ keV. Thus, it is very hard, if not impossible, to reproduce observed non-thermal emission reaching in some cases 10 keV (Uchiyama *et al.* 2003).

In this paper we investigate an alternative possibility that non-thermal X-ray filaments are associated with the contact discontinuity separating ejecta and circumstellar material. We point out that there is a natural way to produce small scale near-equipartition magnetic fields in young (pre-Sedov) SNRs due to the *dynamical compression of magnetic fields at the contact discontinuity*, see Section 2. This possibility has already been noted by Kulsrud *et al.* (1965), who considered the expansion of the ejecta in a medium of constant density and constant magnetic field, and by Rosenau *et al.* (1976) (see also Lee and Chen 1968), who considered the propagation of magneto-hydrodynamic shocks into an ideal gas permeated by a current-free toroidal magnetic field (for a relativistic wind this has been done by Lyutikov 2002).

While the progenitors of core-collapse supernovae blow bubbles into the ambient medium, their wind carries magnetic flux with it. After the explosion, the supernova ejecta propagates through the wind-blown bubble, sweeping magnetic flux with it. A fraction of the swept-up magnetic flux piles up the contact discontinuity, where the magnetic field reaches equipartition with the thermal flow. Similarly, the reverse shock sweeps up magnetic flux of the ejecta, part of which piles up on the contact discontinuity.

The distinct possibility that the thin X-ray filaments are associated with the contact discontinuity may resolve the inconsistencies of the forward shock acceleration model listed above.

- Since there is no flow of material across the contact discontinuity, there is no problem with the advection of accelerated electrons. Our estimates of the diffusion rate show that the diffusion length in one synchrotron decay time is short enough to be consistent with the thickness of filaments.
- High values of the magnetic field decrease electron diffusion away from the sheath. In addition, since the region of high magnetic field is small, the synchrotron emissivities are small outside of the sheath.
- Near the contact discontinuity the background plasma consists of both circumstellar medium and ejecta, which is enriched with heavy elements. Acceleration and the associated thermal heating may occur on both sides of the contact discontinuity (in the ejecta and in the circumstellar material).
- It is feasible, though we do not demonstrate it, that plasma acceleration mechanisms are more efficient than standard shock acceleration.
- A large ratio of TeV to synchrotron emitting volumes is a natural consequence of the magnetic field compression.

2. Magnetic fields of young SNRs

The expansion of SN ejecta into the circumstellar medium has been the subject of numerous studies (see, *e.g.* , Truelove & McKee 1999 for the latest review), so that the hydrodynamic behavior is well understood. The dynamic effects of the magnetic field have been largely ignored, though. For the typical magnetic field this is a justified assumption *except* near the contact discontinuity separating the shocked ejecta and the circumstellar medium.

The dynamics of the shocked wind strongly depends on whether the explosion is in the Sedov phase or in the ejecta-dominated phase, when the piled-up mass is still smaller than the ejecta mass, *i.e.* at times $t \leq E^{-1/2} M_{ej}^{5/6} \rho_0^{-1/3}$ (*e.g.* Truelove & McKee 1999), where E is the energy of the explosion, M_{ej} is the ejecta mass, and ρ_0 is the external density. In the Sedov phase, most of the shocked circumstellar material and, due to the "frozen-in" condition, the magnetic field is concentrated in a thin layer near the shock surface. On the other hand, in the ejecta-dominated phase the presence of the contact discontinuity between the circumstellar material and ejecta changes the dynamics considerably. In particular, for a wide variety of ejecta and wind profiles the plasma density formally diverges on the contact discontinuity. On account of the frozen-in condition, this means that the magnetic field diverges as well (Kulsrud *et al.* 1965; Rosenau 1975; Rosenau & Frankenthal 1976). The reverse shock propagating in the ejecta leads to a similar, perhaps even more prominent, effect (Hamilton & Sarazin 1984). *Thus, no matter how weak the preshock magnetic field is, there is always a thin boundary layer near the contact discontinuity where the magnetic pressure is comparable to or even dominates over the kinetic pressure.* The thickness of the layer depends on the wind and the ejecta magnetic field. Exact solutions (*e.g.* Rosenau 1975) indeed show that on the contact discontinuity the pressure is provided solely by the magnetic field, and the kinetic pressure vanishes. [2]

Next we outline the dynamics near the contact discontinuity (for details see Rosenau & Frankenthal 1976). Assume that the ejecta is propagating through a cold supersonic magnetized wind with a constant velocity v_0 and a decreasing mass density $\rho \propto r^{-2}$ (this is expected for a supersonically moving pre-supernova wind). Let the speed of the forward shock be v_s. The assumption of a cold plasma implies that the sonic Mach number is infinity. In the wind the magnetic field is expected to be dominated by the toroidal component $B_\phi \propto 1/r$, so that the Alfvén velocity, $v_A = B/\sqrt{4\pi\rho}$, remains constant. We will parameterize the strength of the magnetic field by the Alfvén Mach number $M_A = (v_s - v_0)/v_A \sim v_s/v_A$, where we assume $v_s \gg v_0$. Note that in case of the Solar wind the Alfvén velocity is somewhat smaller, but comparable to the terminal velocity $v_A \leq v_0$. After the passing of the forward shock the magnetic field and the particle density are compressed by the factor $(\gamma + 1)/(\gamma - 1) = 4$. At the same time the post-shock pressure is $p \sim \rho v_s^2 \gg B^2/4\pi$, so that the post-shock plasma is strongly dominated by the kinetic pressure. Thus, *in the bulk* of the shocked flow dynamic effects of magnetic field are mostly negligible (see,

[2] A similar effect occurs for the interacting winds case (Emmering & Chevalier 1987)

though, Chevalier & Luo 1994), but it cannot be neglected in a narrow sheath near the contact discontinuity.

To estimate the width of the magnetized sheath in the swept-up circumstellar medium we need to specify the motion of the shock and can then use the solutions of Rosenau & Frankenthal (1976). For simplicity, we assume here that the SNR is well in the ejecta-dominated regime. In this case, the velocity of the shock is constant $v_s = \text{const}$, while the structure of the shocked wind is self-similar, depending only on $\xi = r/R_S$, where R_S is the shock position at a given time. The contact discontinuity is located at $\xi_{CD} \simeq 0.78$. For large Alfvén Mach numbers $M_A \gg 1$ the flow dynamics far from the contact discontinuity follows the hydrodynamical case. In the vicinity of the contact discontinuity the dynamical behavior is complicated, though. In the absence of a magnetic field the kinetic pressure remains constant, while the density tends to infinity and the temperature to zero. For an adiabatic index $\gamma = 5/3$ the three quantities obey the following scaling relations in $\hat{\xi} = \xi - \xi_{CD} \ll 1$:

$$p = \text{const.}, \qquad \rho \sim \hat{\xi}^{-4/9} \to \infty, \qquad T \sim \hat{\xi}^{4/9} \tag{1}$$

If the flow carries a small magnetic field, then the frozen-in condition requires

$$B \sim \rho \sim \hat{\xi}^{-4/9} \to \infty \tag{2}$$

Therefore, however small the magnetic field is, it becomes dynamically important near the contact discontinuity. Thus the flow may be separated into a bulk flow, where the magnetic field is dynamically not important, and a magnetized sheath where its pressure is comparable to the kinetic pressure. In the magnetized sheath

$$p \sim \hat{\xi}^{4/3}, \qquad \rho \sim \text{const.}, \qquad B = B_0 = \text{const.}, \qquad T \sim \hat{\xi}^{4/3} \tag{3}$$

Since the magnetic field on the CD should transport all the momentum from the ejecta, B_0 will be of the order of the equipartition pressure.

The width of the magnetized layer, ΔR_{sheath}, is

$$\Delta\zeta \simeq \frac{\Delta R_{\text{sheath}}}{R} \simeq M_A^{-9/4} \tag{4}$$

It may be shown that only a small fraction $\sim M_A^{-5/4}$ of the total swept-up flux is concentrated near the contact discontinuity. Most of the swept-up flux is still near the shock surface, for in the ejecta-dominated phase the self-similar solutions for the forward shock have similar properties as in the Sedov phase. Though most of the magnetic flux is distributed near the shock surface, the magnetic field near the contact discontinuity is $\sim M_A$ times higher, so that for a homogeneous electron distribution the synchrotron emissivity is M_A^2 times higher near the contact discontinuity. The synchrotron emission produced near the contact discontinuity can thus dominate the total radiation yield, in particular if one observes the sheath edge-on.

To estimate the physical size of the magnetized sheath one must know the parameters of the pre-supernova wind, a highly uncertain and varying quantity. For a Type II SNR remnant

propagating into a wind blown cavity it will depend on whether the forward shock is propagating in the fast, ~ 1000 km /sec WR wind, in the preceding slow wind of the LBV, or in the progenitor stage wind, usually that of an O-star. In all cases the magnetic fields in the wind are virtually unknown (*e.g.* Cassinelli 2001). For a qualitative estimate we assume that the wind is propagating at a few hundred kilometers per second, and the shock velocity of the supernova is several thousand kilometers per second. To estimate the magnetic field we assume that the Alfvén velocity at the sonic point of the wind is of the order of the sound speed and that the terminal velocity of the wind is typically only a few times larger than the velocity at the sonic point. Then the Alfvén Mach number is $M_A \sim 10 - 30$ and $\Delta\zeta \simeq 10^{-2} - 10^{-3}$.

Similarly, it is possible to estimate the thickness of the magnetized sheath in the ejecta using the self-similar solutions of Hamilton & Sarazin (1984). Unfortunately, it crucially depends on the density profile of the ejecta (see, *e.g.* , Truelove & McKee 1999) and also on the even more uncertain value of the magnetic field in the ejecta. Nevertheless, the pile-up of the ejecta magnetic field may be more important than that of the circumstellar medium, for downstream of the reverse shock a larger fraction of the shocked material may pile up on the contact discontinuity, whereas downstream of the forward shock most of the material is still near the shock. For example, in the self-similar solutions of Hamilton & Sarazin (1984), $\rho \propto \hat{\zeta}^{-6/5}$ and the thickness of the magnetized sheath in the ejecta is

$$\Delta\zeta_{ej} \sim M_{A,ej}^{-6/5}, \tag{5}$$

where $M_{A,ej}$ is the Alfvén Mach number of the reverse shock, so that almost all of the magnetic flux, that passed through the reverse shock, piles up on the contact discontinuity.

3. Modeling non-thermal X-ray emission

3.1. Where are the high-energy particles accelerated?

Having established that a thin sheath of high magnetic field strength should exist at the contact discontinuity, we will now discuss possible processes of particle acceleration and the locations thereof, for which two possibilities seem to exist. First, relativistic electrons can be accelerated at the forward shock, but they would not produce high-energy emission efficiently, for the magnetic field is fairly low. As the accelerated electrons are advected downstream and diffuse through the shocked plasma, they will encounter regions of high magnetic field at the contact discontinuity, where they may produce non-thermal X-rays and loose most of there energy. Scenarios invoking a non-linear magnetic field amplification through streaming instabilities of cosmic rays, that have been produced by diffusive shock acceleration at the forward shock (Berezhko, Ksenofontov, & Völk 2003), are apparently disfavored on account of the X-ray spectrum of the filaments (Aharonian & Atoyan 1999, Uchiyama *et al.* 2003).

Secondly, the electrons may be accelerated right in the high magnetic field regions near the contact discontinuity. In this case, the acceleration could not be due to shock acceleration, for there

is no jump in parallel velocity at the contact discontinuity. Alternatively, the particle acceleration may be due to plasma instabilities that develop in a thin magnetized sheath. This, in principle, can be much more efficient. In this section we consider these two alternatives. We construct a model of propagation and synchrotron emission of electrons in an inhomogeneous magnetic and velocity fields that should be present near the contact discontinuity. We find that if electrons are accelerated far from the contact discontinuity, typically too few electrons would diffuse into the high field region near the contact discontinuity to produce bright narrow features, unless the diffusion coefficient is very high.

Before doing detailed calculations let us first make a simple estimate whether the size of the thin filaments is consistent with local acceleration. Let's assume that electrons diffuse out of the high magnetic field regions due to Bohm-type diffusion perpendicular to the magnetic field. Let the diffusion coefficient be parameterized as

$$\kappa_\perp = \lambda r_L c \tag{6}$$

where $r_L = \gamma c/\omega_B$ is the relativistic Larmor radius and $\lambda \leq 1$ (for Bohm diffusion $\lambda = 1$). Then the diffusion scale in one synchrotron decay time, τ_c, is

$$l_{\rm diff} \simeq \sqrt{\lambda r_L \tau_c c} \tag{7}$$

Using the observed size of the filaments we can make an estimate of the magnetic field strength assuming that the filament thickness is due to diffusion and energy losses.

$$\omega_B \simeq \frac{c}{l_{\rm diff}} \sqrt[3]{6\pi\,\lambda\,\frac{l_{\rm diff}}{r_e}} \tag{8}$$

where r_e denotes the classical electron radius. Note, that this estimate is independent of particle energy, so that, if taken at face value, this would imply that all emission (from radio to TeV) should be confined to the filament. For the magnetic field we find

$$B \simeq (150\ \mu{\rm G})\ \lambda^{1/3}\ \left(\frac{l_{\rm diff}}{0.1\ {\rm pc}}\right)^{-2/3} \tag{9}$$

For a given parameter $\lambda \leq 1$ this gives a lower limit to the magnetic field, for the thickness of filaments can be determined not only by diffusive escape, as would have been the case if the acceleration occurred in an infinitely thin region, but also by the physical size of the acceleration region itself.

3.2. Propagation of high-energy electrons

The X-ray filaments observed with *Chandra* satellite in SNRs are very thin compared with the radius of the remnants, and therefore we may treat the propagation of electrons as a one-dimensional problem. If the contact discontinuity propagates outward at a constant velocity, it

is convenient to use a comoving spatial coordinate, z, such that $z = 0$ marks the position of the contact discontinuity at all times. We approximate the energy loss by adiabatic expansion in the spherical outflow by a catastrophic loss term

$$\mathrm{div}\, V = \frac{1}{r^2}\,\frac{\partial}{\partial r}\left(r^2\, V\right)\Big|_{r=R_{\rm CD}} \simeq 2\,\frac{V_{\rm cd}}{R_{\rm cd}}$$

$$\Rightarrow\ -\frac{\partial}{\partial E}\left[\frac{1}{3}\,\mathrm{div}\, V\ E\, N\right] \simeq -\frac{\partial}{\partial E}\left[\frac{2}{3}\,\frac{V_{\rm cd}}{R_{\rm cd}}\,E\,N\right]\ \longrightarrow\ \frac{N}{\tau_{\rm ad}} = \frac{2}{3}\,\frac{V_{\rm cd}}{R_{\rm cd}}\,N \tag{10}$$

For young SNRs like SN 1006 the adiabatic loss time is $\tau_{\rm ad} \approx 10^{11}$ sec, longer than the age of the remnant. In the case of RX J1713.7-3946 the distance may be either $d \simeq 6\,$kpc (Slane *et al.* 1999), implying $\tau_{\rm ad} \approx 10^{12}$ sec and an age a factor of three less, or $d \simeq 1\,$kpc (Koyama *et al.* 1997), in which case $\tau_{\rm ad} \approx 1.8 \cdot 10^{11}$ sec and the age is a factor of six less than that. Thus the adiabatic cooling associated with the spherical expansion of the remnant is probably unimportant in the present phases of expansion for the remnants. On the other hand, the synchrotron loss time scale for synchrotron emission at an X-ray energies is

$$\tau_{\rm syn} \simeq (2 \cdot 10^{10}\ \mathrm{sec})\,\left(\frac{B}{20\ \mu\mathrm{G}}\right)^{-1.5}\,\left(\frac{E_X}{4\ \mathrm{keV}}\right)^{-0.5} \tag{11}$$

so that continuous energy losses by synchrotron emission will not only be important near the contact discontinuity, where the field strength can be very high, but also in the regions toward the forward and reverse shocks.

Under these conditions the dynamics of very high-energy electrons near the rim of a supernova remnant can be reasonably well described by a one-dimensional continuity equation for the isotropic differential number density of relativistic electron, $N(E, z)$, which incorporates the effects of diffusion, convection, adiabatic deceleration, and energy loss terms (Owens & Jokipii 1977)

$$-\frac{\partial}{\partial z}\left[D(E,z)\frac{\partial N}{\partial z} - V(z)N\right] - \frac{\partial}{\partial E}\left[\left(\frac{1}{3}\,\frac{dV}{dz}\,E - \beta(E,z)\right)N\right] = Q(E,z) \tag{12}$$

with appropriate boundary conditions for $N(E, z)$. In Eq.12 $D(E, z)$ is the scalar diffusion coefficient, $V(z)$ is the convection velocity of cosmic-ray electrons relative to the contact discontinuity, $Q(E, z, t)$ represents the source distribution, and $\beta(E, z) = \dot{E}$ is the rate of continuous energy losses. We assume that synchrotron emission is the dominant energy loss process. Then

$$\beta(E,z) = -E^2\, b(z) \tag{13}$$

where the spatial function $b(z)$ is proportional to the square of the magnetic field strength, B^2. The diffusion coefficient is likely near the Bohm limit, for the freshly accelerated, streaming cosmic rays very efficiently excite Alfvén waves (Wentzel 1974; Skilling 1975a; 1975b; 1975c). The diffusion coefficient will therefore decrease as B increases. It thus seems appropriate to set

$$D(E,z) = D(E)\, d(z) = D_0\, E^a\, d(z)\,, \qquad 0 \le a < 1 \tag{14}$$

with the scaling relation

$$d(z)\,b(z) = \alpha = \text{const.} \tag{15}$$

For $a \rightarrow 1$ we can recover the Bohm limit for the diffusion coefficient. Eq.12 can then be rewritten in terms of the new spatial coordinate

$$\mu = \int^z \frac{ds}{d(s)} \tag{16}$$

as

$$-\frac{\partial}{\partial\mu}\left[D(E)\,\frac{\partial N}{\partial\mu} - V(\mu)N\right] - \frac{\partial}{\partial E}\left[\left(\frac{1}{3}\,\frac{dV}{d\mu}\,E + \alpha\,E^2\right)\,N\right] = d(\mu)\,Q(E,z) = Q(E,\mu) \tag{17}$$

where the revised source density $Q(E,\mu)$ is now differential in μ instead of z. $N(E,\mu)$, however, is still differential in z. For the case that the convection velocity relative to the contact discontinuity is linear in the new coordinate μ,

$$V(\mu) = 3\,V_1\,\mu \tag{18}$$

The Green's function, $\mathcal{G}$, which satisfies

$$-\frac{\partial}{\partial\mu}\left[D(E)\,\frac{\partial\mathcal{G}}{\partial\mu} - 3\,V_1\,\mu\,\mathcal{G}\right] - \frac{\partial}{\partial E}\left[\left(V_1\,E + \alpha\,E^2\right)\,\mathcal{G}\right] = \delta\left(E - E'\right)\,\delta\left(\mu - \mu'\right) \tag{19}$$

for homogeneous boundary conditions at infinity, can be found in the literature (Lerche & Schlickeiser 1981, see their Eq. 72) as

$$\begin{aligned}\mathcal{G} \;=\; & \frac{\Theta\left(E' - E\right)}{2\,\sqrt{\pi}\,\left(V_1\,E + \alpha\,E^2\right)}\,\frac{\exp\left(3\,V_1\,\tau(E)\right)}{\left[\int_{\tau(E)}^{\tau(E')} dx\;D(x)\;\exp(6\,V_1\,x)\right]^{0.5}} \\ & \times\;\exp\left(-\frac{\left[\mu\,\exp\left(3\,V_1\,\tau(E)\right) - \mu'\,\exp\left(3\,V_1\,\tau(E')\right)\right]^2}{4\,\left[\int_{\tau(E)}^{\tau(E')} dx\;D(x)\;\exp(6\,V_1\,x)\right]}\right)\end{aligned} \tag{20}$$

where

$$\begin{aligned}\tau(E) &= \int^E \frac{du}{V_1\,u + \alpha\,u^2} \\ D(\tau) &= D\left[\tau(E)\right] = D_0\,E^a\end{aligned} \tag{21}$$

and $\Theta(x)$ is the Heaviside function.

The general properties of this solution have been outlined in Lerche & Schlickeiser (1982) and Pohl & Schlickeiser (1990). Here we will use a specific spatial profile for the magnetic field strength (and for the diffusion coefficient) to describe the propagation of high-energy electrons near to and in the pile-up region around the contact discontinuity of a young SNR. Though the pile-up of the magnetic field appears to be a general property of the systems, the calculations of Rosenau & Frankenthal (1976) suggest that the spatial profile of the magnetic field strength near the contact

discontinuity depends somewhat on the Alfvénic Mach number of the outflow and on the density profile of the upstream medium. We may therefore assume a simple mathematical profile

$$d(z) = \frac{1 + \left(\frac{z}{z_1}\right)^2}{1 + \left(\frac{z}{z_0}\right)^2} \ , \quad z_1 \ll z_0 \tag{22}$$

corresponding to a variation of the magnetic field strength

$$B(z) \propto \sqrt{b(z)} = \sqrt{\alpha \, \frac{1 + \left(\frac{z}{z_0}\right)^2}{1 + \left(\frac{z}{z_1}\right)^2}} \tag{23}$$

The magnetic field is thus assumed to be constant at large distances from the contact discontinuity, $z \gg z_0$. It would increase approximately $\propto z^{-1}$ for $z_1 \ll z \ll z_0$, and is constant again close to the contact discontinuity at $z \ll z_1$ with a value a factor of z_0/z_1 higher than far away from the contact discontinuity.

Then the new spatial coordinate, μ, scales as

$$\mu = \left(\frac{z_1}{z_0}\right)^2 z + \left[1 - \left(\frac{z_1}{z_0}\right)^2\right] z_1 \, \arctan\left(\frac{z}{z_1}\right) \tag{24}$$

The convection velocity, V, is then linearly increasing as $V(z) = 3\,V_1\,z$ for $z \ll z_1$. For $z \gg z_1$ the velocity gradient continuously decreases until it turns constant again for $z \gg z_0$, where $dV/dz = 3\,V_1\,z_1^2/z_0^2$. This velocity profile is in accord with the findings of Rosenau & Frankenthal (1976).

For ease of exposition we will assume the sources of electrons to be located either at the contact discontinuity (case A) or far away from it (case B). The source terms for these two situations are

$$Q_A = q_0 \, \delta(\mu) \, E^{-p} \, \Theta(E_{\max} - E) \tag{25}$$

and

$$Q_B = q_0 \, \delta(\mu - \mu_s) \, E^{-p} \, \Theta(E_{\max} - E) \tag{26}$$

In the high-energy limit $\alpha E \gg V_1$, *i.e.* synchrotron energy losses dominate, the differential number density of electrons then is

$$N = \frac{q_0 \sqrt{1-a} \, E^{-p-\frac{1+a}{2}}}{2\sqrt{\pi \, D_0 \, \alpha}} \int_1^{\frac{E_{\max}}{E}} dx \ \frac{x^{-p}}{\sqrt{1 - x^{a-1}}} \, \exp\left[-\frac{(1-a)\,\alpha}{4\,D_0\,E^{a-1}} \, \frac{(\mu - \mu_s)^2}{1 - x^{a-1}}\right] \tag{27}$$

where $\mu_s = 0$ for sources at the contact discontinuity. In the argument of the exponential function, the factor

$$z_D = \sqrt{\frac{4\,D_0\,E^{a-1}}{(1-a)\,\alpha}} \tag{28}$$

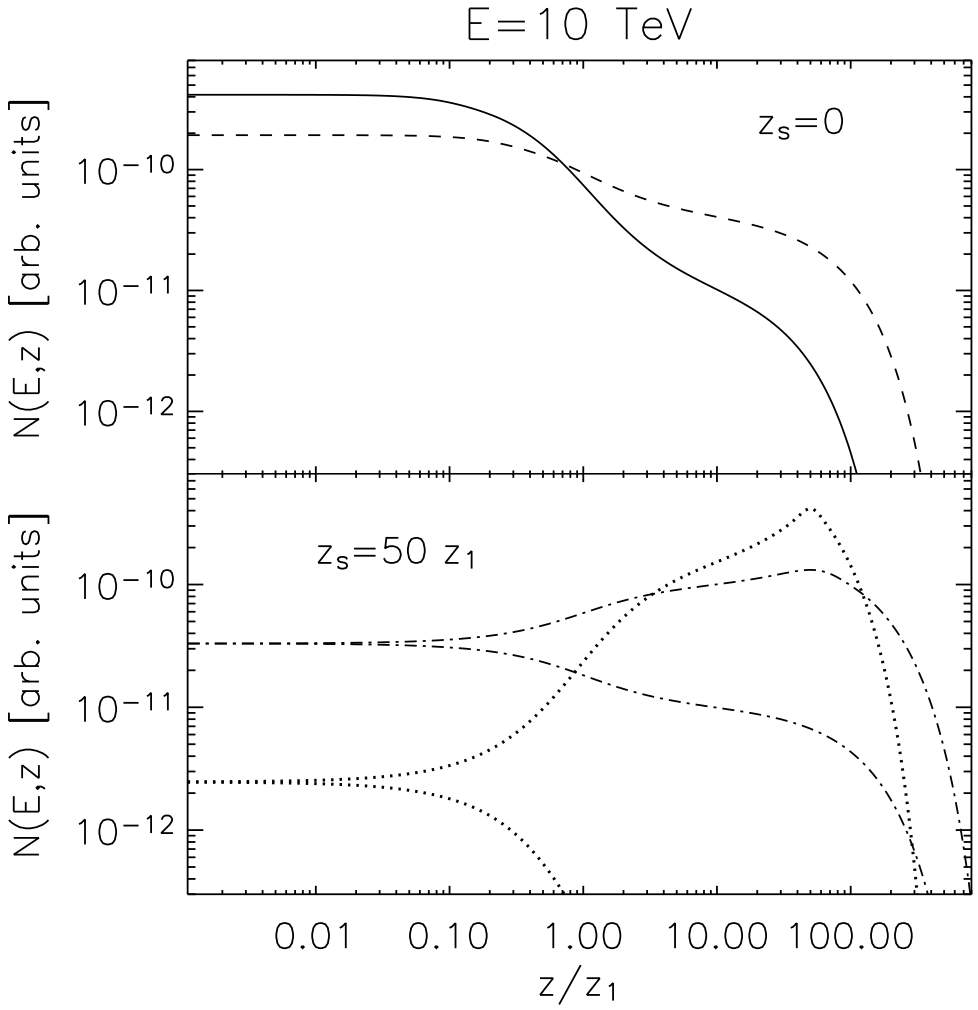

Fig. 1.— The electron flux at $E = 10\,\mathrm{TeV}$ as a function of position for sources at the contact discontinuity (top panel). The solid line indicates the electron flux for the standard parameters listed in Table 1. The electron distribution is symmetric around $z = 0$ for sources at the contact discontinuity. For comparison, with the dashed line we also show the electron distribution derived for a higher diffusion coefficient ($\eta_{\mathrm{Bohm}} = 20$) with smaller energy dependence ($a = 0.6$). The bottom panel shows the electron flux for sources outside of the contact discontinuity at $z_s = 50\,z_1 = 5$ pc, in which case the distribution is not symmetric around $z = 0$ and two profiles must be shown, the higher one applying to the source side of the contact discontinuity and the lower line to the side far from the sources. The dotted lines are for a standard diffusion coefficient and the dash-dotted lines for $\eta_{\mathrm{Bohm}} = 20$, but standard energy dependence $a = 0.9$. Obviously the diffusion coefficient must be very high to transport a copious supply of electrons to the contact discontinuity, where they can efficiently radiate.

is effectively the propagation length within one synchrotron loss time at the contact discontinuity.

In Figure 1 we illustrate the characteristic behavior of the differential electron density. For this purpose we use a standard set of parameters, shown in Table 1, and compare the spectra thus derived with those for a non-Bohmian diffusion coefficient and for electron sources far from the contact discontinuity. For the standard parameters the propagation length $z_D(1\,\mathrm{TeV}) \simeq 3.4\,z_1$. To be noted from the figure is that for sources at the contact discontinuity the width of the spatial distribution of the electron flux falls off much closer to the contact discontinuity than indicated by the propagation length in one loss time, z_D, on account of the additional factor $1/(1-x^{a-1})$ in the argument of the exponential function in Eq.27. For comparison, as the dashed line we also show the electron distribution derived for a higher diffusion coefficient with smaller energy dependence ($a = 0.6$), for which the propagation length is $z_D(1\,\mathrm{TeV}) \simeq 5.4\,z_1$. Though the spatial distribution is clearly wider than for the standard parameters, it also starts rolling off very close to the contact discontinuity.

If the electron sources are located far from the contact discontinuity, e.g. at the forward shock, very few electrons will reside at or be transmitted through the contact discontinuity, unless the diffusion coefficient is very high. With the dash-dotted line we also show the electron distribution derived for a higher diffusion coefficient with $\eta_{\mathrm{Bohm}} = 20$, but standard energy dependence $a = 0.9$, for which the propagation length is $z_D(1\,\mathrm{TeV}) \simeq 10.7\,z_1$. Most high-energy electrons would be located near to the source location.

3.3. The integrated emission spectra

Equipped with the electron flux as a function of location and energy, we can now proceed to calculate the emission properties. We will begin with the volume-integrated spectra at X-ray energies and in the TeV band. We do not know the electron source strength, q_0, and therefore we can not make a prediction for the absolute fluxes. However, we can determine the X-ray and γ-ray fluxes relative to each other, which should be sufficient for the comparison with the multi-band spectrum of individual SNRs. In the simple one-zone models, the TeV-to-X-ray flux scaling is a measure of the magnetic field strength (Pohl 1996). In our spatially inhomogeneous model the situation is more complicated.

In the calculation of the TeV-band γ-ray emission we will consider only the up-scattering of the microwave background, partly because of the Klein-Nishina cut-off and partly because the ambient photon densities in the far-infrared will often be too small to significantly influence the results. In any case, a modeling of the up-scattered infrared emission will require a careful assessment of the infrared photon fields near and in the SNR in question and thus can be performed only for a specific object (e.g. see Atoyan et al. 2000). In the isotropic case, the differential cross section for the scattering of a photon with incident energy ϵ to the energy E_γ by an elastic collision with an

electron of energy E is given by (Blumenthal & Gould 1970)

$$\frac{d\sigma}{d\epsilon}(E_\gamma, \epsilon, E) = \frac{3\,\sigma_T\,m_e^2\,c^4}{4\,\epsilon\,E^2}\,\left[2q\,\ln q + (1+2q)(1-q) + \frac{(1-q)\,(\Gamma_e\,q)^2}{2\,(1+\Gamma_e\,q)}\right] \tag{29}$$

where

$$q = \frac{E_\gamma}{\Gamma_e\,(E-E_\gamma)} \quad \text{and } \Gamma_e = \frac{4\,\epsilon\,E}{m_e^2\,c^4} \tag{30}$$

In our case $\Gamma_e \approx 1$ and thus the Thomson limit is not valid. Given the differential electron number density, $N(E)$, the γ-ray emissivity in the TeV band is calculated as

$$j_\gamma = \frac{c\,E_\gamma}{4\pi}\,\int_{E_{\rm min}} dE\,\int d\epsilon\;n(\epsilon)\,N(E)\,\frac{d\sigma}{dE_\gamma} \tag{31}$$

where

$$n(\epsilon) = \frac{1}{\pi^2\,\hbar^3\,c^3}\,\frac{\epsilon^2}{\exp\left(\frac{\epsilon}{kT}\right)-1} \tag{32}$$

is the blackbody photon density spectrum of the microwave background (with $T = 2.73\,\mathrm{K}$). The total emission spectrum is then calculated as the volume integral of the emissivity, which essentially corresponds to using the volume-integrated electron spectrum in Eq.31.

The corresponding volume integral of the synchrotron emissivity is more complex, for the magnetic field strength, B, varies considerably over the emission region. The volume-integrated X-ray and TeV-band spectra are shown in Fig.2 both for sources at and far from the contact discontinuity, using the same parameter combinations as in Fig.1. To be noted from the figure is that by variation of the propagation length, z_D, one can indeed reduce the keV-to-TeV flux ratio, as was suggested by Allen, Petre & Gotthelf (2001) and Lazendic et al. (2004). However, more important appears the location of the electron sources, for the smallest flux ratio is produced, if the sources are far from the contact discontinuity. In that case most of the synchrotron emission is generated in regions of low magnetic field strength and the X-ray spectrum is correspondingly soft.

Please note that the spectra shown in Fig.2 have been calculated assuming a steady-state situation. While that appears justified at X-ray energies of a few keV or higher, it may be inappropriate for low-energy X-rays. Depending on the age and the acceleration history of the supernova remnant in question, there will be a spectral transition somewhere in the UV or soft X-ray regime from a spectrum at lower energies, that is essentially unaffected by energy losses and just reflects the source spectrum, to a steady-state spectrum at higher energies, that we discuss here. As a consequence, the low-frequency synchrotron spectrum will be harder by a spectral index change $\Delta s = 0.5$ compared with the high-frequency spectrum. A corresponding turnover should be observable in the inverse Compton spectrum at TeV energies. This spectral feature arises from the relation between the electron energy loss time and the age of the system, and it has nothing to do with the usual energy loss limits on the maximum achievable energy in the electron acceleration process. The typical electron spectrum will have a cut-off and a spectral break, the former being the consequence of the energy limit of the electron acceleration, and the latter being caused by

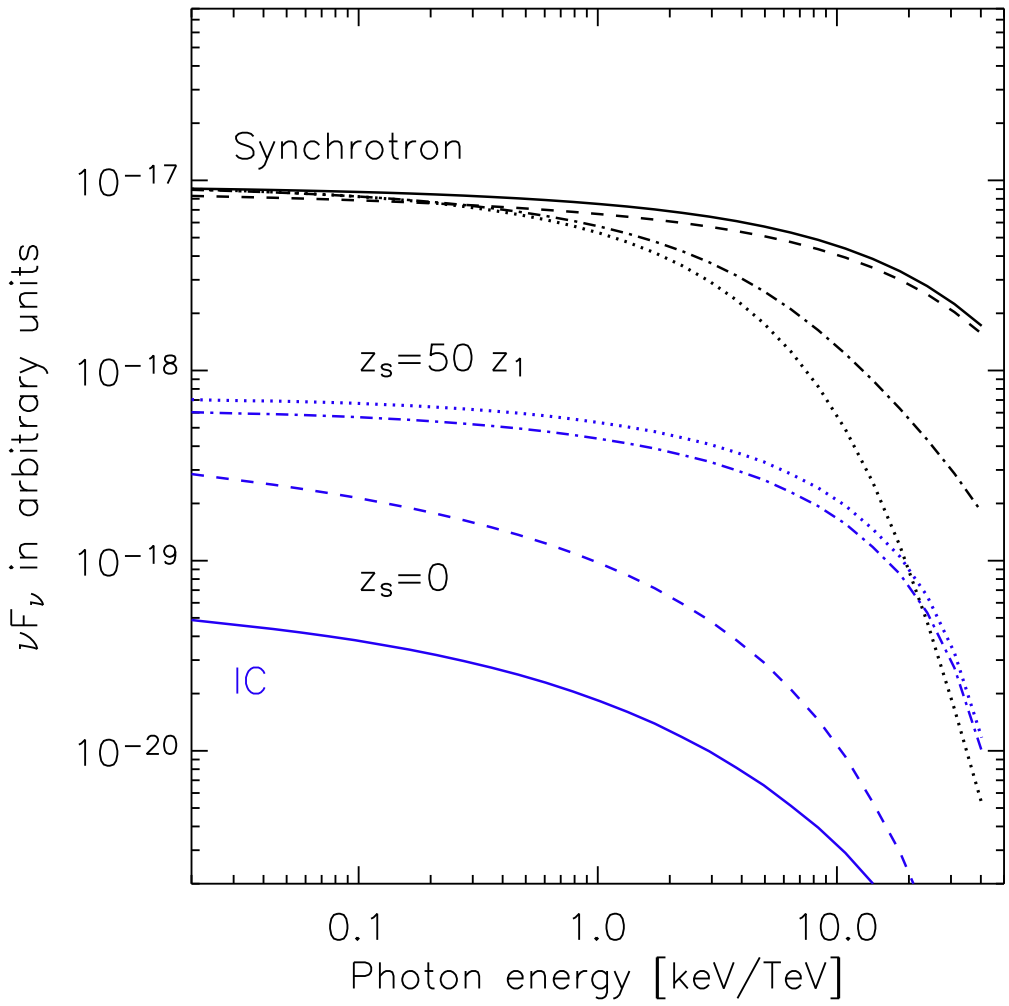

Fig. 2.— The volume-integrated emission spectra at X-ray energies (by synchrotron emission) and in the TeV band (by inverse Compton scattering). The fluxes are in arbitrary units but obey the correct relative scaling. The relation between the linestyles and the parameters used are as in Fig.1. The abscissa units are keV for the synchrotron emission and TeV for the inverse Compton spectra.

the transition from the pure source spectrum at low energies to a steady-state situation at higher energies. A radiation modeling of SNRs based on simple power-law spectra with cut-off is therefore inappropriate.

3.4. X-ray filaments: the intensity profile at the contact discontinuity

While the curvature of the contact discontinuity appeared negligible in the treatment of the electron propagation, this is clearly not the case when discussing X-ray intensity profiles at the contact discontinuity. The observable intensity distribution will be different from the spatial profile of the synchrotron emissivity, j_X, as a function of the distance from the SNR center, r. Assuming spherical symmetry of the SNR we can calculate line-of-sight integrals of X-ray intensity in the energy interval $[E_1, E_2]$ as

$$I_X(r_0) = \int_{E_1}^{E_2} dE_X \; E_X^{-1} \int_{-\infty}^{\infty} dx \; j_X \left(E_X, r = \sqrt{r_0^2 + x^2} \right) \tag{33}$$

where r_0 is the distance between the line-of-sight and the center of the remnant. The observable intensity distribution (Eq.33) will depend on our choice of diffusion coefficient, $\eta_{\rm Bohm}$, source location, z_s, and thickness of the magnetic pile-up region, z_1. To solve this line-of-sight integral we also need to specify the radius of the contact discontinuity, $r_{\rm CD}$, for in the preceding calculations we have used a spatial coordinate z with the contact discontinuity as the origin, so that now $r = r_{\rm CD} + z$. The resulting profiles for the parameters given in Table 1 and $r_{\rm CD} = 10\,{\rm pc}$ are shown in Fig.3 for the typical X-ray energy band 3-10 keV. To be noted from the figure is the large difference between the intensity scale length upstream and downstream of the contact discontinuity. For the standard parameters (the solid line) the downstream scale length is approximately a factor of seven larger than upstream. The dotted lines refer to electron sources far from the contact discontinuity and apparently the magnetic field pile-up does not cause a corresponding enhancement in the X-ray intensity. Thus it seems that the high-energy electrons must be produced close to or at the contact discontinuity to explain the narrow X-ray filaments.

Also apparent in Fig.3 is that extended diffuse emission may be observed far from the contact discontinuity, the intensity of which downstream and upstream depends on the source location and the diffusion coefficient.

How does the filament width scale with the parameters, such as the width of the pile-up region, z_1, the diffusion coefficient, $\eta_{\rm Bohm}$, or the source location, z_s? The intensity profile near the contact discontinuity seems to have a variety of shapes, depending on where the electron sources are located, and thus one measure of filament width doesn't do justice to all situations. With that limitation in mind, we have calculated the distance from the point, where the intensity in the 3-10 keV band is at its peak value, to the location, where it has fallen to $1/e$ of that, and use the quantity thus derived as the thickness scale length l_e of the X-ray filament. Obviously l_e will be different upstream and downstream of the contact discontinuity on account of its spherical geometry and possibly the

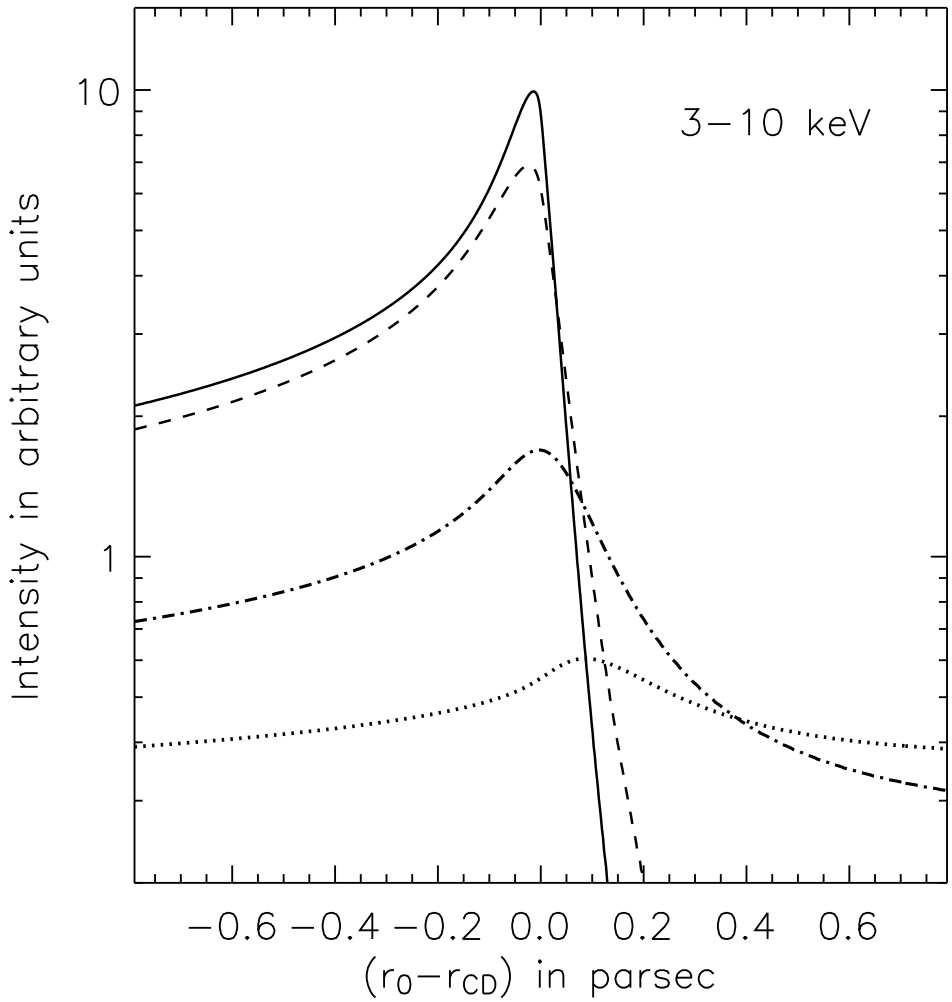

Fig. 3.— The X-ray intensity distribution in the 3-10 keV energy band as seen by an outside observer assuming spherical symmetry of the SNR (Eq.33). The different linestyles correspond to the same sets of parameters as in Fig.1. Only if the electron sources are close to or at the contact discontinuity (solid and dashed lines), a narrow enhancement or filament would be observed in the X-ray intensity profile.

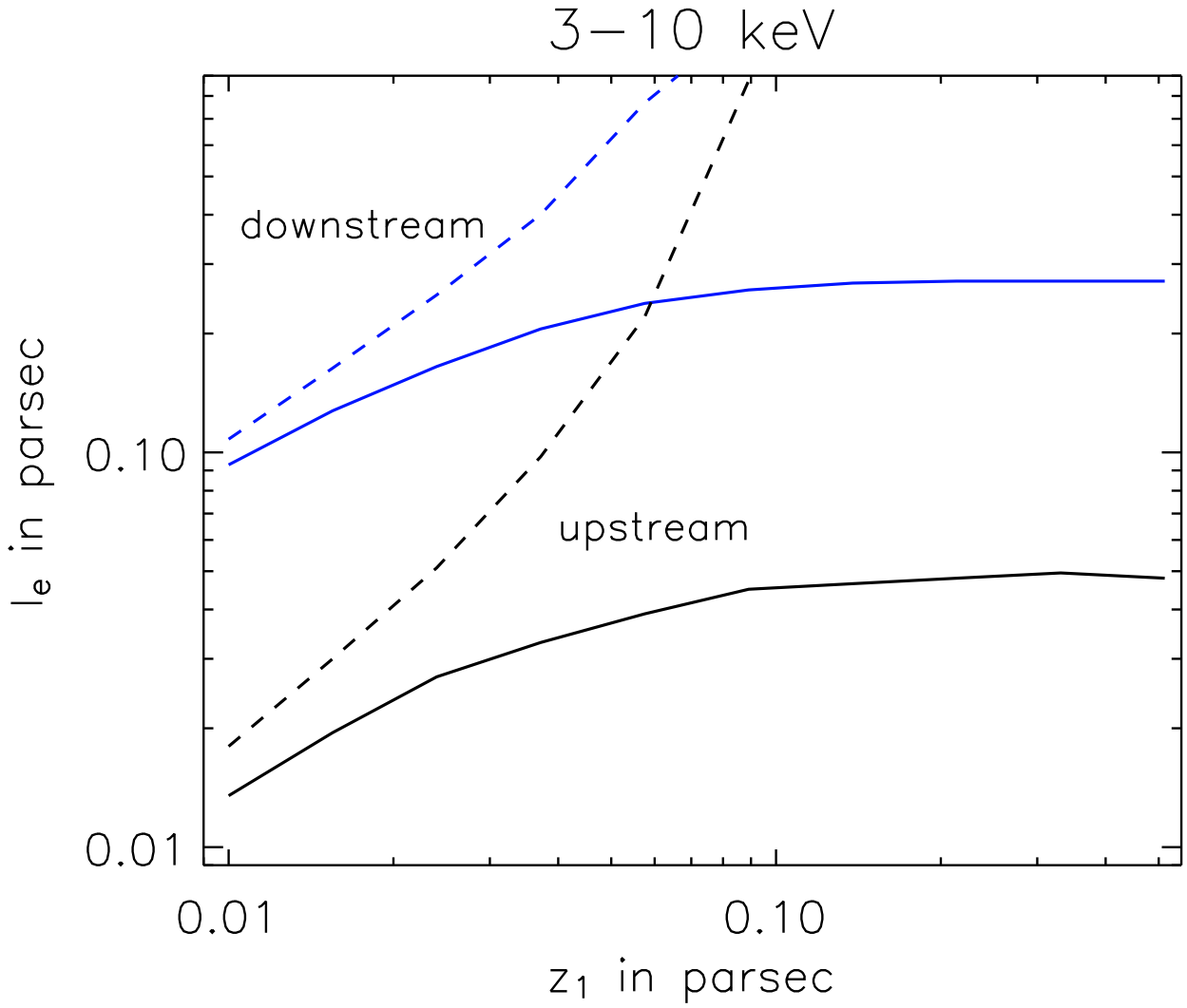

Fig. 4.— The exponential scale length for the 3-10 keV band, l_e, upstream and downstream of the contact discontinuity, here plotted as a function of the thickness of the magnetic field pile-up region, z_1. The solid lines refer to the standard values for all other parameters, whereas the dashed lines are for a source location outside of the pile-up region at $z_s = 20\, z_1$.

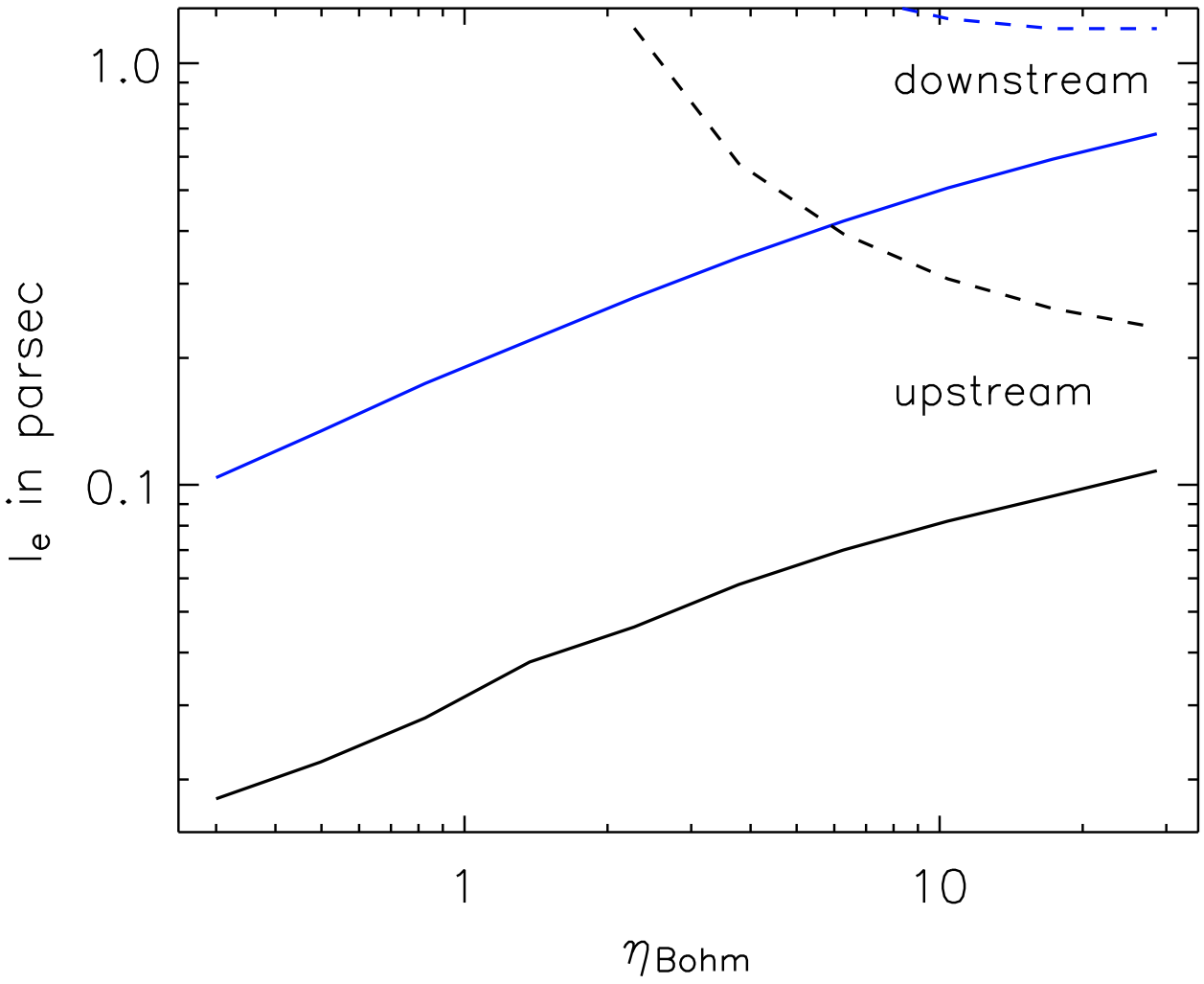

Fig. 5.— The exponential scale length for the 3-10 keV band, l_e, displayed as a function of the diffusion coefficient in units of its Bohm limit, $\eta_{\rm Bohm}$. The linestyles and their relation to the parameters are as in figure 4.

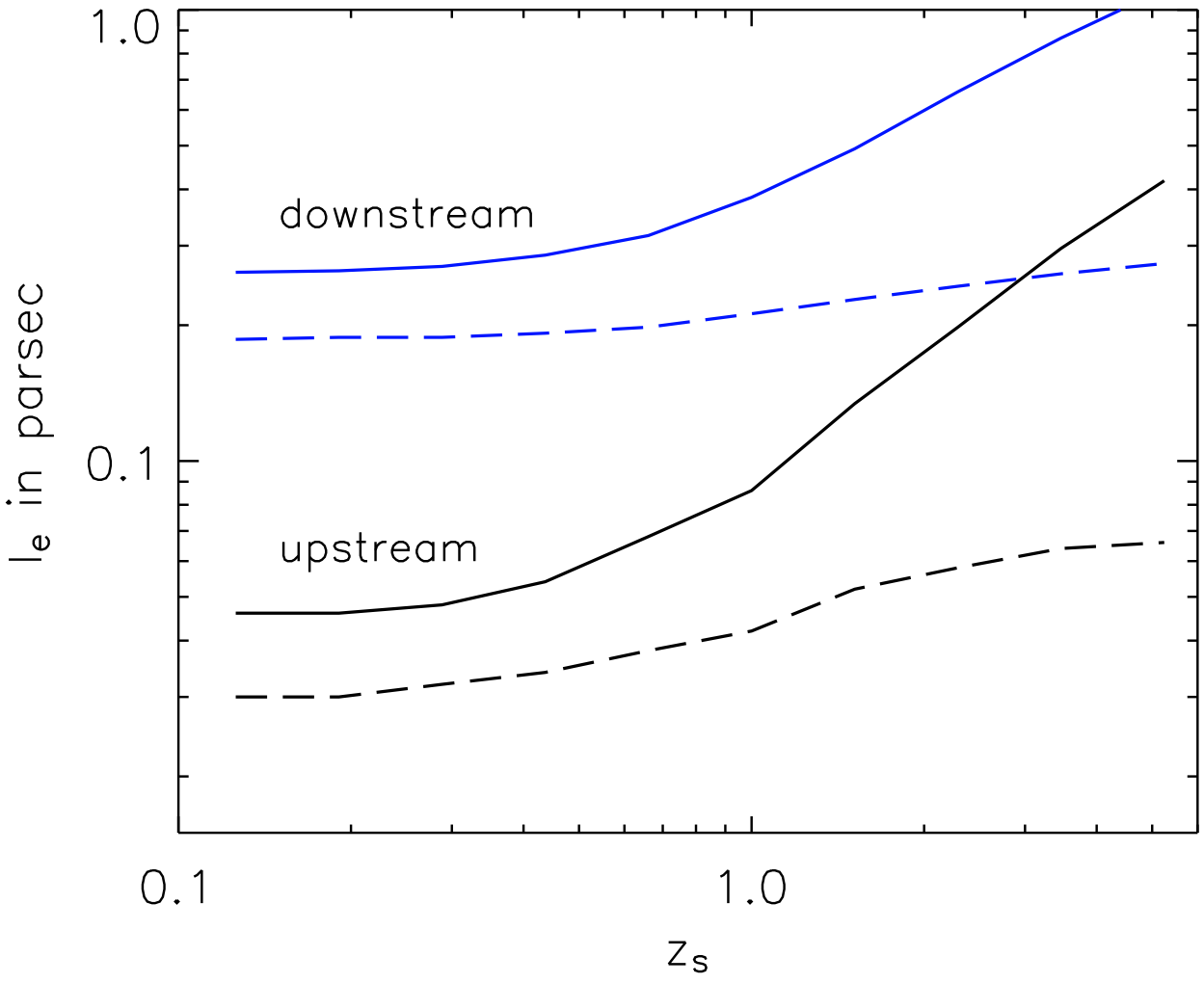

Fig. 6.— The exponential scale length for the 3-10 keV band, l_e, shown versus the electron source location, z_s. Again, the solid lines refer to the standard values for all other parameters, whereas the dashed lines are for a reduced width of the magnetic pile-up region, $z_1 = 0.03$ pc.

electron source location.

In the figures 4, 5, and 6 we show the thickness scale length, l_e, as a function of the thickness of the magnetic field pile-up region, z_1, in dependence of the diffusion coefficient, $\eta_{\rm Bohm}$, and versus the electron source location, z_s, respectively, while in each case all the other parameters have been kept at their standard values as listed in table 1.

To be noted from Fig.4 is that very thin X-ray filaments can be produced whatever the source location, if the thickness of the magnetic field pile-up region, z_1, is very small, though much less magnetic flux is compressed at the contact discontinuity in that case. However, only for electron sources at the contact discontinuity the thickness of the X-ray filaments remains small even for high values of z_1. The scale length, l_e, turns constant for large z_1, because the energy losses do no longer permit the high-energy electrons to fully occupy the region of enhanced magnetic field. For $z_1 \gtrsim 0.03$ pc narrow filaments will not be observed, if the electron sources are far from the contact discontinuity.

If one increases the diffusion coefficient from values below the Bohm limit, the filament thickness will also increase. However, Fig.5 indicates that the increment in the scale length l_e is less than that in the propagation length scale $z_D(\propto \sqrt{\eta_{\rm Bohm}})$. Thus, both the thickness of the magnetic pile-up region and the electron diffusion coefficient must be sufficiently small to produce narrow X-ray filaments, if the radiating electrons are produced at the contact discontinuity. For electron sources far from the contact discontinuity (indicated by the dashed line), the diffusion coefficient must be large enough to allow a significant fraction of the electrons to propagate to the high magnetic field region around the contact discontinuity, otherwise narrow filaments will not be observed.

Fig.6 shows that if the electron sources are not located in the magnetic pile-up region around the contact discontinuity anymore ($z_s > 1$), two things will happen unless the thickness of the pile-up region is very small (this case is indicated by the dashed lines): firstly, the width of the X-ray filaments will substantially increase, in fact approximately linearly with z_s in case of the upstream length scale. Secondly, whereas for $z_s \approx 0$ the intensity length scale l_e downstream is roughly a factor of 5 larger than that upstream of the contact discontinuity, the two length scales tend to get closer to each other with increasing z_s.

Summarizing our results on the X-ray scale length we note that if the electron sources are located far from the contact discontinuity, only for a sufficiently thin magnetic pile-up region with $z_1 \lesssim 0.03$ pc can narrow X-ray filaments with a downstream exponential length scale $l_e \lesssim 0.3$ pc be observed. On the other hand, if the electrons are accelerated at the contact discontinuity, narrow X-ray filaments would be produced for a broad variety of diffusion coefficients and widths of the magnetic field sheath. We therefore conclude that if the X-ray filaments are caused by magnetic field pile-up at the contact discontinuity, it is much more likely that the relativistic electrons are locally accelerated than far from the contact discontinuity.

We have also searched for spectral differences between the X-ray intensity of the filaments and that of the extended downstream regions. For that purpose we have defined the filament region as

the area, in which the 3-10 keV band integrated intensity is higher than half of its maximum. The downstream region then extends from the filament to 1 pc away from the contact discontinuity. The filament intensity and plateau intensity are just averages over the areas in question,

$$I_{\rm fil} = \frac{1}{l^+_{1/2}+l^-_{1/2}} \int_{r_{CD}-l^-_{1/2}}^{r_{CD}+l^+_{1/2}} dr_0\ I_X(r_0) \tag{34}$$

$$I_{\rm pla} = \frac{1}{[1\,{\rm pc}]-l^-_{1/2}} \int_{r_{CD}-[1\,{\rm pc}]}^{r_{CD}-l^-_{1/2}} dr_0\ I_X(r_0) \tag{35}$$

electron In Fig.7 we show the ratio of these intensity spectra for the same four sets of parameters that we have used in the Figures 1-3. If the spectral form of the emission from the filaments and the plateau regions was the same, the lines would be flat at a value defined by the jump in the mean intensity. Excluding the case of sources far away and a small diffusion coefficient, in which filaments are only marginally existent, all curves have a positive slope, thus indicating that the filament spectra seem to be slightly harder than those of the downstream region. However, the difference in spectral index is with $\Delta\alpha \lesssim 0.05$ probably too small to be observable. In the case of RX J1713.7-3946 claims of spectral constancy (Uchiyama *et al.* 2003) have been published. Care must be exercized, though, for there is a clear ambiguity in spectral fits related to the absorbing column density and the emission spectral index. The spectral constancy reported by Uchiyama *et al.* (2003) requires that the absorbing column is highest toward the regions of highest intensity, which seems unlikely. Keeping the absorbing column fixed in the spectral analysis, Lazendic *et al.* (2004) find the X-ray spectra of the filaments harder than those of the plateau emission.

4. Magnetic dissipation at the contact discontinuity?

Can dissipation of the magnetic field power the non-thermal X-ray emission? If we estimate the total X-ray luminosity of a typical young SNR to be $10^{35}-10^{36}$ erg/sec and a typical age 10^3-10^4 yrs, then the total emitted energy over the life time is $\lesssim 10^{47}$ ergs, or about 0.01% of the total mechanical energy of a SNR, $E_{\rm tot}$. The energy in the non-thermal component should be smaller than the total free energy available for particle acceleration.

The total energy associated with the magnetic field in the sheath can be estimated as

$$E_{sheath} \sim \frac{\Delta R_{sheath}}{R} E_{tot} \sim \frac{E_{tot}}{M_A^{9/4}} \sim \left(10^{-2}-10^{-3}\right)\ E_{tot} \sim 10^{48}{\rm ergs}, \tag{36}$$

This estimate (36) implies that the total X-ray energetics of SNRs is only slightly less than the total magnetic energy of the swept-up material. In addition, the magnetic field of the ejecta will contribute to the nonthermal emission as well, but its contribution cannot be estimated due to the unknown values of the magnetic field in the ejecta. [3]

[3]There is a renewed interest in magnetically-driven SN explosion, stimulated by the association of some SN with

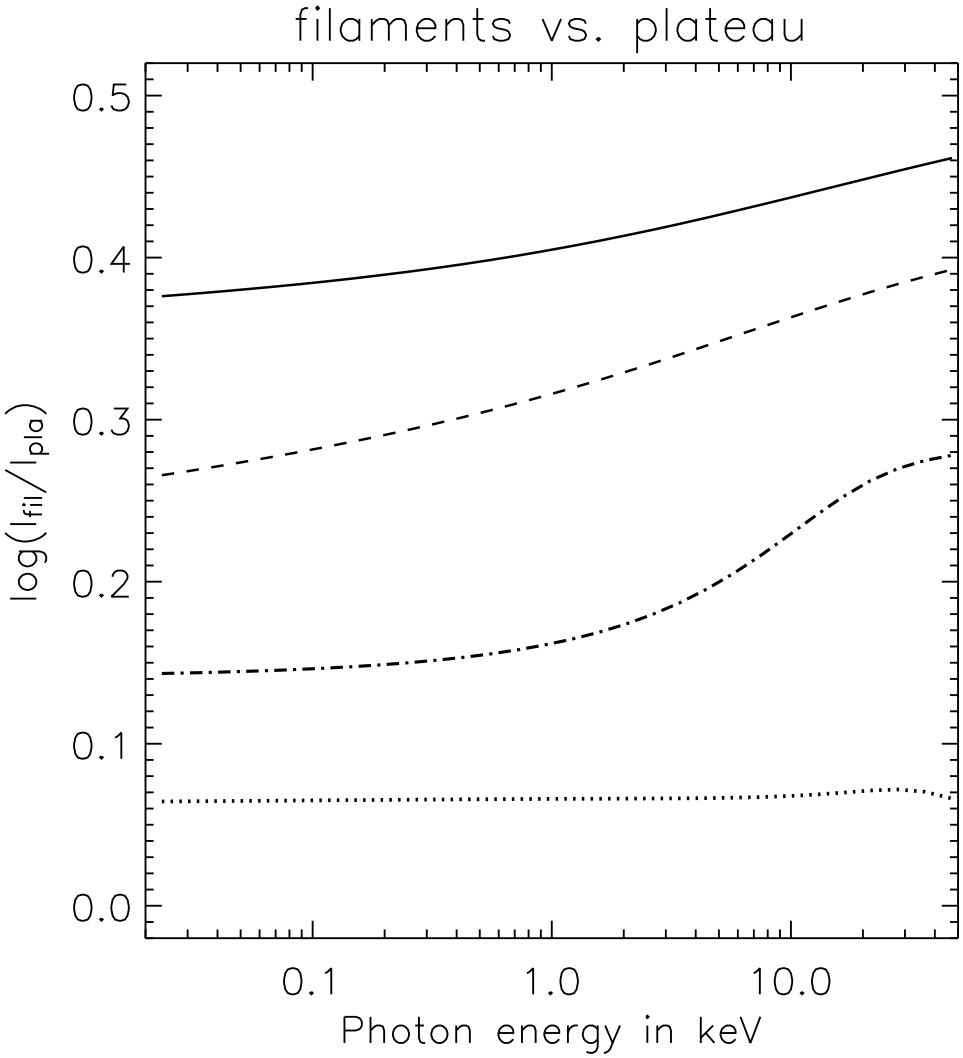

Fig. 7.— The ratio of the average X-ray intensities of the filaments and the extended downstream regions according to Eq.35, shown as a function of the photon energy. Here 'filament' is defined by the X-ray intensity in the 3-10 keV band being at least 50% of the peak value. The downstream spectrum is derived in the region between the filament and 1 pc away from the contact discontinuity, i.e. a bit further than what is shown in Fig.3. The filament spectra seem to be slightly harder than those of the downstream region, if with a spectral index difference of $\Delta\alpha \lesssim 0.05$ probably too little to be detectable. The relation between the linestyles and the parameters used are as in Fig.1.

One possible mechanism for the energy transfer from a magnetic field to relativistic particles is magnetic reconnection in the compression region at the contact discontinuity. Note, that the contact discontinuity is, in fact, a rotational discontinuity of magnetic field, so that there are current flowing along it. Dissipation of those currents may, in principle, power the non-thermal emission. Magnetic reconnection leads to a large-scale DC electric field which efficiently accelerate particles either directly, or through generation of MHD turbulence (*e.g.* Priest & Forbes 2000). The accelerating electric field can be parameterized as $E = \xi B$, $\xi \leq 1$ (this is equivalent to acceleration on a time scale $t_{acc} \sim \xi\gamma/\omega_B$; in a framework of reconnection models (*e.g.* , Priest & Forbes 2000) $\xi = v_{in}/c$ where v_{in} is the inflow velocity). Balancing the acceleration rate with the synchrotron energy loss rate, we find for the maximum Lorentz factor, $\gamma_{\rm max}$, and the energy of the corresponding synchrotron photons, $E_{\rm max}$,

$$E_{X,\,\rm max} = \xi\,\frac{27}{8}\,\frac{m\,c^2}{\alpha}$$
$$\gamma_{\rm max} = \frac{3}{2}\,\sqrt{\xi\,\frac{m\,c^3}{e^2\,\omega_B}} \tag{37}$$

where α is the fine structure constant. Then, in order to have the observed X-ray synchrotron emission in the ~ 5 keV range one requires

$$\xi > \alpha\,\frac{8}{27}\,\frac{E_X}{m\,c^2} \simeq 2\cdot 10^{-5}\,\left(\frac{E_X}{5\ {\rm keV}}\right) \tag{38}$$

There will be other loss processes, e.g. associated with scattering on magnetic turbulence, that will limit the efficacy of acceleration and hence may require a value of ξ larger than calculated here. Nevertheless, values of $\xi \ll 1$ may be sufficient to accelerate electrons such that they can emit X-ray synchrotron radiation.

The treatment of magnetic dissipation is notoriously complicated and has little predictive power (see, e.g., Lesch & Pohl 1992). For example on cannot calculate ξ from first principles. In this section our intention was to point out the consistency of basic back-of-the-envelope estimates for the total energetics and the acceleration rates with the notion that non-thermal X-ray emitting electrons may be accelerated at the contact discontinuity.

5. Discussion

We have investigated the possibility that the non-thermal X-ray filaments observed in pre-Sedov SNRs are related to the dynamical compression of magnetic field at the contact discontinuity that separates the circumstellar medium and the ejecta. The pile-up of magnetic field at the contact discontinuity has been extensively studied in the literature (Kulsrud *et al.* 1965; Lee & Chen 1965;

GRBs.

Rosenau 1975; Rosenau & Frankenthal 1976). We have combined the magnetohydrodynamical structure of magnetized outflows as described in these publications with a one-dimensional diffusion-convection transport equation to describe the propagation of non-thermal electrons near the contact discontinuity of a young SNR and to calculate spatially resolved emission spectra in the X-ray and TeV bands. We have considered two possible acceleration regions: one in the low field region far from the contact discontinuity, and the other at the contact discontinuity.

As a result we find that the X-ray intensity distribution will depend strongly on the electron diffusion coefficient and on the thickness of the magnetized sheath at the contact discontinuity. If the electron sources are located far from the contact discontinuity, only for a sufficiently thin magnetic pile-up region with thickness $z_1 \lesssim 0.03$ pc can narrow X-ray filaments with a downstream exponential length scale $l_e \lesssim 0.3$ pc be observed. On the other hand, if the electrons are accelerated at the contact discontinuity, narrow X-ray filaments would be produced for a broad variety of diffusion coefficients and widths of the magnetic field sheath. We therefore conclude that if the X-ray filaments are caused by magnetic field pile-up at the contact discontinuity, it is much more likely that the relativistic electrons are locally accelerated than far from the contact discontinuity.

We have also calculated the volume-integrated X-ray synchrotron and TeV-band inverse Compton spectra with a view to thoroughly investigate the expected *gamma*-ray flux. In the case of RX J1713.7-3946, measurements taken with the CANGAROO experiment suggest a TeV-band spectrum (Enomoto *et al.* 2002), that cannot be readily understood as inverse Compton emission, but also not as hadronic in origin (Reimer & Pohl 2002). If the γ-ray emission volume was very much larger than the X-ray emission volume, the inverse-Compton interpretation of the TeV-band spectrum would again be tenable (*e.g.* Pannuti *et al.* 2003).

Depending on the location of the electron acceleration site, as well as on the diffusion coefficient and the thickness of the magnetized sheath at the contact discontinuity, the TeV-to-keV flux ratio can vary by more than an order of magnitude. A relatively high TeV flux is observed either if the diffusion coefficient is very large or if the radiating electrons are accelerated far from the magnetic pile-up region, *e.g.* at the forward shock. These situations are exactly those, for which narrow X-ray filaments can be observed only if the magnetized sheath at the contact discontinuity is very thin with $z_1 \lesssim 0.03$ pc. Thus, the conditions favorable for the occurrence of thin X-ray filaments have little overlap with those causing a relatively high TeV flux. We have assumed a magnetic field strength $B = 10$ μG far from the contact discontinuity, and find that even under favorable circumstances the TeV energy flux is still an order of magnitude lower than the keV energy flux, which is insufficient to explain the TeV-band spectrum of RX J1713.7-3946 observed with CANGAROO. The magnetic field is already compressed by the forward shock, and a lower field strength, that in principle may reduce the discrepancy, seems therefore unlikely. Furthermore, in cases of high TeV flux the TeV-band spectrum is typically hard in comparison with the X-ray spectrum, also in contrast to the measurements. We therefore feel, that our model does not offer a comprehensive explanation for the CANGAROO measurements of RX J1713.7-3946.

Dynamical compression of magnetic field at the contact discontinuity generically happens in the pre-Sedov stage, which may explain why non-thermal filaments appear both in Type II and in Type Ia supernova. The particular appearance of filaments and their relative importance in producing X-rays may depend on the progenitor. Core collapse SN are preceded by several stages of wind-related mass loss, during which a considerable amount of magnetic flux is expelled. After the SN explosion the wind's magnetic field is then compressed at the contact discontinuity. This is applicable to Cas A, and RX J1713.7-3946. On the other hand, SN 1006 was probably Type Ia event (Winkler *et al.* 2003) and thus is not expected to have a considerable wind-blown nebular around it. Explosions into the interstellar medium are expected to produce very thin magnetized sheaths, with a thickness $\Delta R/R \sim M_A^{-3}$ (Kulsrud *et al.* 1965), so that only a fraction M_A^{-2} of the swept-up flux is concentrated at the contact discontinuity. In this case, the magnetic flux from the SN progenitor itself, dynamically compressed at the *inner* side of the contact discontinuity, may be more important than the field of the circumstellar material (*e.g.* Lou 1994).

One of the arguments in favor of a forward-shock interpretation of the filaments in SN 1006 is that their position coincides with the H_α rim. H_α emission often occurs at shock fronts due to both charge exchange reactions and collisional heating. One may expect that, if particles are accelerated at the contact discontinuity, this should be accompanied by plasma heating, similar to Solar flares. This, in principle, can produce H_α emission as well if there is atomic hydrogen present near the contact discontinuity.

As the SNR becomes older, it evolves from the ejecta-dominated to the Sedov-dominated phase. During this evolution the contact discontinuity slows down its motion, receding further from the forward shock, and is finally pushed back to smaller radii (*e.g.* Truelove & McKee 1999). As the contact discontinuity recedes from the shock, smaller and smaller amounts of the magnetic flux are concentrated on it. In addition, if the forward shock becomes radiative, the amount of the magnetic flux piled on the contact discontinuity decreases even further, as radiative shock have larger compression ratios, so that less flux is advected downstream. Thus, the non-thermal emission will subside after the SNRs either enter the Sedov phase or the forward shock becomes radiative.

The location of the contact discontinuity should vary as the expanding SNR collides with inhomogeneities caused by the progenitor's wind or structure in the interstellar medium, thus producing a complicated structure. In addition, the contact discontinuity may be unstable with respect to Rayleigh-Taylor and Richtmyer-Meshkov processes (Kane *et al.* 1999). A stretching of the toroidal magnetic field by density clumps and by instabilities may explain why radio polarization studies indicate that projected large-scale magnetic fields tend to be oriented in the radial direction (*e.g.* Reynolds & Gilmore 1993).

6. Acknowledgements

We would like to thank Felix Aharonyan, Roger Blandford, Roger Chevalier, Steve Reynolds and Chris Thompson. ML acknowledges support by NSERC grant RGPIN 238487-01. MP acknowledges support by NASA under award No. NAG5-13559.

REFERENCES

Aharonian, F. A. *et al.* . 2001a, A&A, 370, 112

Aharonian, F. A. *et al.* . 2001b, A&A, 373, 292

Aharonian, F. A. *et al.* . 2002, A&A, 395, 803

Allen, G.E., Petre, R., and Gotthelf, E.V., 2001, ApJ, 558, 739

Allen, G. E. *et al.* , 1997, ApJ, 487, 97

Atoyan, A.M., Aharonian, F.A., Tuffs, R.J., and Völk, H.J., 2000, A&A, 355, 211

Bamba, A., Koyama, K., and Tomida, H., 2000, PASJ, 52, 1157

Bamba, A., Yamazaki, R., Ueno, M., Koyama, K., 2003, ApJ, 589, 827

Bell, A.R. & Lucek, S.G., 2001, MNRAS, 321, 433

Berezhko, E.G, Ksenofontov, L.T., and Völk, H.J. , 2002, A&A, 395, 943

Berezhko, E.G., Pühlhofer, G., and Völk, H.J. , 2003, A&A, 400, 971

Berezhko, E.G., Ksenofontov, L.T., and Völk, H.J. , 2003, A&A, 412, L11

Blumenthal, G.R. & Gould, R.J., 1970, Rev. Mod. Phys., 42-2, 237

Borkowski, K.J., Rho, J., Reynolds, S.P., and Dyer, K.K. , 2001, ApJ, 550, 334

Buckley, J.H., et al., 1998, A&A, 329, 639

Cassinelli, J.P., 2001, in *Observable Effects of B Fields on the Winds and Envelopes of Hot Stars*, ASP Conf. Ser. 248, Mathys, G., Solanki, S. K., Wickramasinghe, D. T., Eds, 651

Chevalier, R. A. & Luo, D., 1994, 421, 225

Chevalier, R. A. & Oishi, J., 2003, ApJ, 593, L23

Emmering, R. T. & Chevalier, R. A., 1987, ApJ, 321, 334

Enomoto, R. *et al.* , 2002, Nature, 416, 823

Gotthelf, E.V., Koralesky, B., Rudnick, L., Jones, T.W., Hwang, U., and Petre, R., 2001, ApJ, 552, 39

Hamilton, A.J.S. & Sarazin, C.L., 1984, ApJ, 281, 682

Kane, J., Drake, R.P., and Remington, B.A., 1999, ApJ, 511, 335

Koyama, K., Petre, R., Gotthelf, E.V., Hwang, U., Matsuura, M., Ozaki, M., and Holt, S.S., 1995, Nature, 378, 255

Koyama, K. *et al.* , 1997, PASJ, 49, 7

Kulsrud, R.M., Bernstein, I.B., Krusdal, M., Fanucci, J. and Ness, N., 1965, ApJ, 142, 491

Lazendic, J.S., Slane, P.O., Gaensler, B.M., et al., 2004, ApJ, in press, astro-ph/0310696

Lee, T.S. & Chen, T., 1965, Planet. Space Sci, 16, 1483

Lerche, I., Schlickeiser, R., 1981, ApJS, 47, 33

Lerche, I., Schlickeiser, R., 1982, A&A, 107, 148

Lesch, H. & Pohl, M., 1992, A&A, 254, 29

Lou, Y., 1994, ApJ, 428, 21

Lucek, S.G. & Bell, A.R., 2000, MNRAS, 314, 65

Lyutikov, M., 2002, Physics of Fluids, 14, 963

Muraishi, H., Tanimori, T., Yanagita, S., *et al.* , 2000, A&A, 354, L57

Owens, A.J. & Jokipii, J.R., 1977, ApJ, 215, 685

Pannuti, T.G., Allen, G.E., Houck, J.C., and Sturner, S.J. , 2003, ApJ, 593, 377

Pohl, M., 1996, A&A, 307, L57

Pohl, M. & Schlickeiser, R., 1990, A&A, 234, 147

Priest, E. & Forbes, T., 2000, *Magnetic reconnection : MHD theory and applications*, Cambridge University Press

Reynolds, S.P. & Gilmore, D.M., 1993, AJ, 106, 272

Rho, J., Dyer, K.K., Borkowski, K.J., and Reynolds, S.P. , 2002, ApJ, 581, 1116

Rosenau, P., 1975, Ph.D. Thesis, Tel Aviv University, Ramat Aviv, Israel

Rosenau, P. & Frankenthal, S., 1976, Phys. Fluids, 19, 1889

Skilling, J., 1975, MNRAS, 172, 557

Skilling, J., 1975, MNRAS, 173, 245

Skilling, J., 1975, MNRAS, 173, 255

Slane, P., Hughes, J.P., Edgar, R.J., Plucinsky, P.P., Miyata, E., Tsunemi, H., and Aschenbach, B., 2001, ApJ, 548, 814

Slane, P., et al., 1999, ApJ, 525, 357

Tanimori, T., et al., 1998, ApJ, 497, 25

Truelove, J.K. & McKee, C.F., 1999, ApJS, 120, 299

Uchiyama, Y., Aharonian, F.A., Takahashi, T., 2003, A&A, 400, 567

Vink, J., 2004, Adv. Sp. Res., in press, astro-ph/0304176

Vink, J. & Laming, J.M., 2003, ApJ, 584, 758

Wentzel, D.G., 1974, ARA&A, 12, 71

Winkler, P.F., Gupta, G., and Long, K.S., 2003, ApJ, 585,324

Table 1. Standard parameters used to derive the figures and their alternative values. The numbers are not standard in the sense of being typical for young SNR, but rather one specific set that we use to demonstrate the typical behavior of the electron distribution and the emission spectra. $B_{\rm far}$ is the magnetic field strength far from the contact discontinuity. The magnetic field at the contact discontinuity is a factor z_0/z_1 stronger. z_s denotes the location of the electron sources, a indicates the energy dependence of the diffusion coefficient, $D \propto E^a$, and $\eta_{\rm Bohm}$ is the diffusion coefficient at E=1 TeV at the contact discontinuity in units of the Bohm diffusion coefficient.

	standard		alternative
z_1	0.1	pc	
z_0	10	z_1	
$E_{\rm max}$	100	TeV	
$B_{\rm far}$	10	μG	
z_s	0		50 z_1
a	0.9		0.6
$\eta_{\rm Bohm}$	2		20